





# Plasma-beta Modulated Characteristics of Magnetohydrodynamic Waves around the Heliospheric Current Sheet

Hui Li<sup>1,2</sup> , Nianwang Li<sup>1,3</sup>, Chi Wang<sup>1,3</sup>, and Shuo Yao<sup>4</sup> 

<sup>1</sup> State Key Laboratory of Space Weather, National Space Science Center, CAS, Beijing, 100190, People's Republic of China; [hli@nssc.ac.cn](mailto:hli@nssc.ac.cn), [linianwang@outlook.com](mailto:linianwang@outlook.com)

<sup>2</sup> University of Chinese Academy of Sciences, Beijing, 100049, People's Republic of China

<sup>3</sup> College of Earth and Planetary Sciences, University of Chinese Academy of Sciences, Beijing, 100049, People's Republic of China

<sup>4</sup> School of Geophysics and Information Technology, China University of Geosciences (Beijing), Beijing, 100083, People's Republic of China

Received 2019 December 20; revised 2019 December 30; accepted 2020 January 8; published 2020 January 22

## Abstract

The magnetohydrodynamics (MHD) wave modes in the heliospheric current sheet (HCS) and the associated heliospheric plasma sheet (HPS) have not been comprehensively investigated in the literature. Based on a frequency-related identification approach, the properties of MHD waves are investigated during 154 HCS crossings observed by the *Wind* spacecraft from 1995 to 2013. Statistically, the incidence of MHD waves around HCS/HPS is found to be modulated by the plasma  $\beta$  within the HPS: (1)  $\beta > 5$ , both Alfvén and slow waves obviously decay within the HPS, with the occurrence rate (OR) decreasing from 60% and 20% in the upstream/downstream to 41% and 14% in the HPS vicinity, respectively; (2)  $1 < \beta \leq 5$ , the OR of Alfvén waves (AWs) remains nearly stable. However, more slow waves are generated after the HCS crossing, with OR increasing from 13% in the upstream/downstream to 22%; (3)  $\beta \leq 1$ , the OR of Alfvén and slow waves remains at  $\sim 58\%$  and 20% during the entire crossing, in spite of some irregular fluctuations. The results for the HCS without a clear HPS are similar to the situations of a low  $\beta$  HPS. The parametric decay instability of AWs is proposed as being responsible for the more slow waves generated in the moderate  $\beta$  HPS, and some indirect observational clues are also given.

*Unified Astronomy Thesaurus concepts:* [Solar wind \(1534\)](#); [Interplanetary magnetic fields \(824\)](#); [Interplanetary physics \(827\)](#); [Magnetohydrodynamics \(1964\)](#); [Alfvén waves \(23\)](#)

## 1. Introduction

The heliospheric current sheet (HCS) embedded within the slow solar wind separates the global oppositely directed open heliospheric magnetic fields (HMF) that originate from the Sun (Schulz 1973; Smith 2001). The region with the same polarity of the interplanetary magnetic field (IMF) is called the sectoral region, and the interface between the sectors is known as the sector boundary (SB; Ness & Wilcox 1964, 1965). Ideally the HCSs should always match with the SB. The heliospheric plasma sheet (HPS) is found to be often associated with the HCS, and is identified by the features of enhanced proton density and plasma beta ( $\beta$ ) (Winterhalter et al. 1994).

Statistically, the width of the HCS at 1 au is generally 10,000 km, about one thirtieth of that of the HPS (Winterhalter et al. 1994; Smith 2001). In this situation, considering the solar wind speed of  $400 \text{ km s}^{-1}$ , it takes only 25 s for a spacecraft to cross a typical HCS, while it takes about 15 minutes (sometimes 30 minutes to an hour) for an HPS. Crooker et al. (2004) found that the three features (SB, HPS, and HCS) do not always appear simultaneously. Winterhalter et al. (1994) and Liu et al. (2014) found that HPSs can straddle, lead, or follow HCSs. Owens et al. (2013) further demonstrated five configurations of HCS and SB. In the most common case the HCS is accompanied by an SB, because the IMF is frozen in the solar wind.

Mostly originating from the Sun, Alfvén waves (AWs) are rarely damped and are observed as the dominant magnetohydrodynamics (MHD) wave mode in the solar wind (Belcher & Davis 1971; Tu & Marsch 1995). The compressive MHD fluctuations, such as fast waves (FWs) and slow waves (SWs), seem unlikely to exist in the solar wind plasma due to strong Landau damping (Barnes 1966; Barnes & Hung 1972;

Barnes 1979). However, local generation mechanism still allows the fast/slow waves be observed at 1 au (Shi et al. 2015). Due to the interaction between small-scale waves and large-scale shear velocity or magnetic field gradients (Roberts et al. 1992; Veltri et al. 1992), a variety of MHD waves are expected to evolve in the HCS and the associated HPS.

Indeed, rich MHD fluctuations, fine-scale discontinuities and small-scale layered structures are observed during the crossing of HCS and HPS by some case studies (Behannon et al. 1981; Crooker et al. 1993; Owen et al. 2005; Blanco et al. 2006; Foullon et al. 2009). Foullon et al. (2009) observed many Alfvénic fluctuations around the HCS through a comparative study of multiple satellites. Smith & Zhou (2007) first reported the existence of SWs in the HPS when the *Ulysses* spacecraft was close to its aphelion at 5 au. In addition, Dai et al. (2014) further presented FWs, accompanied with the phase-steeped edge of a large-amplitude AWs in the HCSs.

In addition to a few observational studies, some numerical models have been used to investigate the evolution of Alfvénicity (degree of correlation between velocity and magnetic field fluctuations) in the presence of a large-scale current sheet. Based on 2D/3D numerical models of MHD turbulence, Roberts et al. (1991, 1992) and Stribling et al. (1996) demonstrated that the Alfvénicity is progressively reduced around the HCSs. By using a 2.5D MHD numerical simulation, Malara et al. (1996, 1997) studied the interaction between AWs and HCSs. They found that Alfvénic fluctuations were weakened but magnetosonic waves were strengthened during HCS crossings, which is probably due to the parametric decay instability (PDI) of an AW (Galeev & Oraevskii 1963; Sagdeev & Galeev 1969; Derby 1978; Goldstein 1978). Furthermore, the compressive fluctuations differ with plasma

beta values. PDI describes how forward-propagating compressive fluctuation is generated and a backward-propagating AW is also produced by the mother forward AW. The growth rate of PDI is given by Galeev & Oraevskii (1963) and Sagdeev & Galeev (1969) as

$$\gamma/\omega_0 = \frac{1}{3\beta^{1/4}}\delta B/B_0 \quad (1)$$

where  $\omega_0$  is the angular frequency of the mother wave,  $B_0$  and  $\delta B$  is the mean value and fluctuation of magnetic field, respectively.

Nevertheless, the MHD waves in the HCS/HPS have not been comprehensively investigated for statistical purposes in the literature. On one hand, the study of MHD fluctuations and subsequent potential wave-mode conversion is helpful to understand plasma heating and turbulence evolution in the solar wind (Chandran & Hollweg 2009; Cranmer & van Ballegoijen 2012; He et al. 2015; Shi et al. 2015). On the other hand, the existence of wave-mode conversion in the magnetotail current sheet (Du et al. 2011) inspires us to perform a statistical study of MHD waves during HCS crossings. In this Letter, we apply a frequency-related identification approach to investigate the MHD wave distribution and potential conversion mechanism around HCS/HPS, and pay more attentions to the effects of plasma beta value.

## 2. Data Sets and Methodology

MHD waves are identified based on the magnetic field and plasma data in the solar wind using the *Wind* spacecraft from 1995 to 2013. All the data is in geocentric solar ecliptic (GSE) coordinates with the temporal resolution of 3 s (Lepping et al. 1995; Lin et al. 1995). The suprathermal electron pitch-angle distribution functions provided by the *Advanced Composition Explorer* (ACE) spacecraft are used to diagnose the HCSs.

### 2.1. Diagnosis of HCS/HPS

HCS separates sectors of inward and outward HMF. Similar to Peng et al. (2017), several criteria are applied to identify HCSs to avoid local current sheets: (1) the magnetic field changes sign and maintains the new polarity for more than half a day; (2) rapid changes in the HMF direction ( $\phi_B$ , the angle of HMF to the X-axis in GSE reference frame) from 135° to 315°, or vice versa; (3) a true SB provided by the Wilcox Solar Observatory (<http://wso.stanford.edu/SB/SB.Svalgaard.html>) is in the vicinity. Note that some events with multiple polarity changes within several hours or the polarity change lasting for more than half an hour are excluded to make the statistical survey focus on typical HCSs. Based on the above criteria, 154 HCSs are identified using the *Wind* observations from 1995 to 2013. Moreover, our results are well consistent with the HCS list of 1995 given by Crooker et al. (2004) and of 2007 given by Peng et al. (2017).

Traditionally, the structures with enhanced proton density, depressed magnetic field strength, and increased plasma beta around HCSs are identified as HPSs (Winterhalter et al. 1994; Smith 2001). In this research, we continue to apply this criterion for the diagnosis of HPS. However, there are no quantitative criteria used in the literature. For practice, we check each HCS to search for HPSs by eye.

### 2.2. Detection of MHD Waves

Correlations between solar wind velocity and Alfvén velocity are often used to identify the Alfvénic fluctuations. However, such a diagnosis method is not valid when there exists some dynamic structures or the background magnetic field is varying. To reduce the uncertainties introduced in determining the background magnetic field and the deHoffmann–Teller frame, the approach by using the bandpass-filtered signals of plasma velocity and magnetic field observations proposed by Li et al. (2016b) are used to identify Alfvén fluctuations. The Walén relation is checked as follows:

$$\delta V_i = \pm \delta V_{Ai}. \quad (2)$$

Here,  $\delta V_i$  and  $\delta V_{Ai}$  represent the band-passed  $V$  (solar wind velocity) and  $V_A$  (local Alfvén velocity) for the  $i$ th filter, respectively. The  $-/+$  signs, respectively, denote the propagation parallel and anti-parallel to the background magnetic field. This approach also helps us to understand the frequency information of fluctuations, which is not available in previous methods. The parameter proposed by Li et al. (2016b),  $Err$ , is used to assess the goodness of the degree of the Alfvénicity, which is the mean value of the following eight parameters: (1)  $|\gamma_c| - 1$ ; (2)  $|\gamma_{cx}| - 1$ ; (3)  $|\gamma_{cy}| - 1$ ; (4)  $|\gamma_{cz}| - 1$ ; (5)  $|\sigma_{\delta V}/\sigma_{\delta V_A} - 1|$ ; (6)  $|\sigma_{\delta V_x}/\sigma_{\delta V_{Ax}} - 1|$ ; (7)  $|\sigma_{\delta V_y}/\sigma_{\delta V_{Ay}} - 1|$ ; (8)  $|\sigma_{\delta V_z}/\sigma_{\delta V_{Az}} - 1|$ . Here, the  $\gamma_c$  is the correlation coefficient between the fluctuations ( $\delta$ ) of plasma velocity ( $V$ ) and Alfvén velocity ( $V_A$ ), and  $\sigma$  represents the standard deviation. Compared to previously used parameters, likely the Alfvén ratio, the Walén slope, the normalized cross helicity, the normalized residual energy, and the velocity-magnetic field correlation coefficient,  $Err$  is a more comprehensive and reliable quantity to represent the Alfvénicity as shown in Li et al. (2016a, 2016b, 2016c, 2017).

As for FWs and SWs, most of previous studies rely on the positive and negative correlation between the magnetic perturbations ( $\delta B$ ) and solar wind number density perturbations ( $\delta N_{SW}$ ). However, such an approach cannot distinguish slow waves, mirror-mode waves, and pressure balance structures from each other. Zhang et al. (2015) and He et al. (2015) used the additional correlation between  $\delta V_{\parallel}$  (fluctuation of velocity component in the direction parallel to the background magnetic field) and  $\delta N_{SW}$  to identify slow waves and additional correlations between  $\delta V_{\perp}$  (fluctuation of velocity component in the direction perpendicular to the background magnetic field) and  $\delta N_{SW}$  to identify fast waves.

Thus, in this study, the detection steps of MHD waves are listed as follows.

- (1) Extracting the low-passed signals of magnetic field ( $B$ ) to obtain the background magnetic field,  $B_0$ . The frequency is between 0 and 1/4000 Hz.
- (2) Calculating the components of velocity in the direction of background magnetic field ( $V_{\parallel}$  and  $V_{\perp}$ ) through the transformation of the coordinate system. Note that, the time resolutions of  $B_0$ ,  $V_{\parallel}$  and  $V_{\perp}$  are always 3 s.
- (3) Extracting band-passed signals of  $V$ ,  $V_A$ ,  $N_{SW}$ ,  $V_{\parallel}$  and  $V_{\perp}$ . For practice, the filters are chosen to be 15–25, 25–40, 40–60, 60–100, 100–160, 160–250, 250–400, 400–630, and 630–1000 s.
- (4) The fragments with  $Err < 0.3$  for three or more filters are marked as AWs.

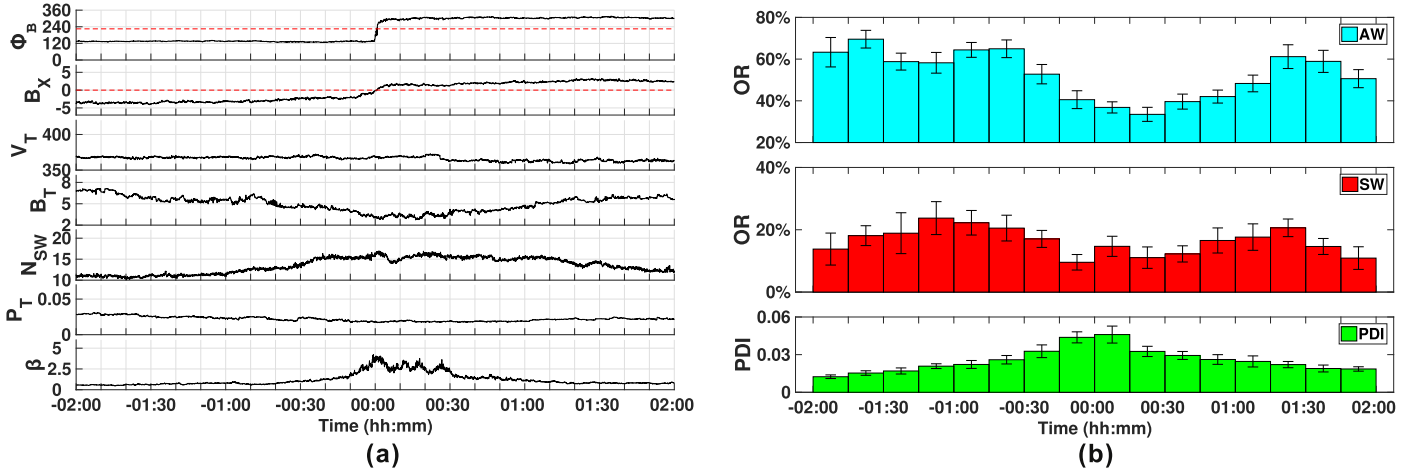


**Figure 1.** Results of the superposed epoch analysis for the HCS crossings with a high  $\beta$  HPS. (a) Overview of the HCS crossing; (b) distribution of the occurrence rate (OR) of MHD waves. The onset of HCS crossing is defined as the epoch time 00:00. The black vertical line represents the data variations,  $\pm\sigma$  (standard deviation).

- (5) The fragments with both correlation between  $\delta B$  and  $\delta N_{SW}$  greater than 0.9 and the absolute value of correlation between  $V_{\perp}$  and  $\delta N_{SW}$  greater than 0.9 for three or more filters are marked as fast waves.
- (6) The fragments with both correlation between  $\delta B$  and  $\delta N_{SW}$  less than  $-0.9$  and the absolute value of correlation between  $V_{\parallel}$  and  $\delta N_{SW}$  greater than 0.9 for three or more filters are marked as slow waves.

Based on such detection criteria, the AWs and fast waves during the HCS analyzed by Dai et al. (2014) can also be well identified but are not shown here.

### 3. Statistical Results

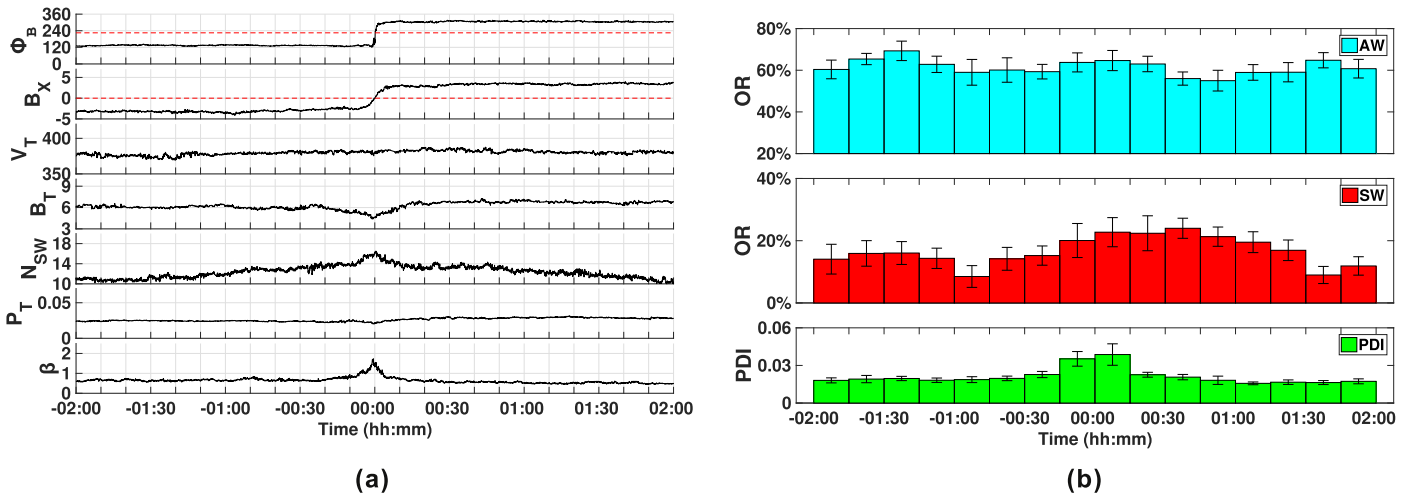
In this study, more focus is placed on investigating the effect of plasma  $\beta$  on MHD wave properties and the potential wave mode conversion mechanism during HCS crossings. For 154 HCS crossings, 30 events are found not to be associated with a clear HPS signature, giving a ratio of 19.5%, which is similar to 25.7% given by Crooker et al. (2004). According to the averaged plasma  $\beta$  of the HPS, the rest 124 HCSs associated with an HPS structure can be further divided into three categories: (1) with a high  $\beta$  HPS,  $\beta > 5$ ; (2) with a moderate  $\beta$  HPS,  $1 < \beta \leq 5$ ; (3) with a low  $\beta$  HPS,  $\beta \leq 1$ . The case number (proportion) for these three categories is 50 (32.5%), 55 (35.7%), and 19 (12.3%), respectively. Note that the maximum 15 minutes averaged value during the HPS is used for this  $\beta$  criterion.

Figure 1 shows the results of superposed epoch analysis for the HCS crossings with a high  $\beta$  HPS. Figure 1(a) gives an overview of the HCS crossing. From top to bottom, the panel gives the medians of HMF direction angle ( $\phi_B$ ), the  $X$  component of magnetic field in the GSE coordinates ( $B_X$  in nT), the solar wind speed ( $V_T$  in  $\text{km s}^{-1}$ ), the magnetic field intensity ( $B$  in nT), the solar wind number density ( $N_{SW}$ ), the total pressure of solar wind ( $P_T$  in nPa), the plasma  $\beta$ , and the growth rate of PDI ( $\gamma/\omega_0$ ), respectively. The onset of HCS crossing is defined as the epoch time 00:00. Note that a mirroring data process is sometimes performed to make the  $B_X$  change from anti-sunward to sunward.  $\phi_B$  sharply changes from  $125^\circ$  to  $335^\circ$  and holds the values for more than two hours. Accordingly,  $B_X$  suddenly changes from  $-3.1$  to  $2.2$  nT and keeps the polarity. These signatures indicate a typical HCS

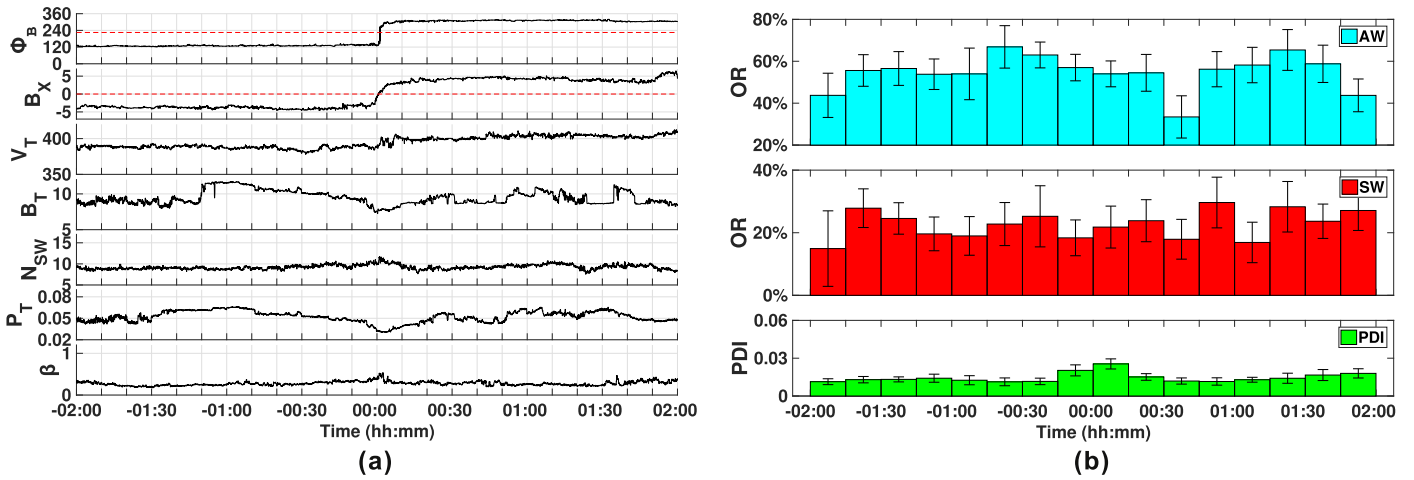
crossing. The solar wind speed remains stable about  $366 \text{ km s}^{-1}$  during the entire HCS crossing, and no clear velocity shears are found. Between  $-00:50$  and  $01:20$ , the simultaneous decrease of  $B_T$  (from 5.8 to 4.2 nT) and enhancement of  $N_{SW}$  (from 11 to  $15 \text{ cm}^{-3}$ ) and  $\beta$  (from 0.7 to 2.0) indicate the existence of a clear long-duration HPS around the HCS crossing. The total pressure keeps constant for the entire HCS crossing. Note that, the superposed  $\beta$  is less than 5 because HPSs can either straddle, lead, or follow HCSs as pointed out by Winterhalter et al. (1994) and Liu et al. (2014).

Figure 1(b) gives the distribution of the occurrence rate (OR) of MHD waves and the growth rate of PDI. The upper panel is for the outward-propagating AWs, and the middle panel represents for the SWs. The bottom panel gives the growth rate of PDI. An interesting finding is that both the OR of Alfvén and slow waves decline within the HPS. In the upstream/downstream, the OR of Alfvén and slow waves is about 60% and 20%. While in the HPS vicinity, it regularly decreases to 41% and 14%, respectively. The physical mechanism of these findings is not clear. PDI is found to be more likely triggered in the HPS, with the growth rate significantly enhanced and peaking in the HPS, which might be responsible for the faster decay of Alfvén waves. De Moortel et al. (2004) found that the velocity perturbations of slow waves decrease with  $\beta$ , implying that a larger  $\beta$  may possibly result in a faster decay of slow waves. However, their conclusions were obtained when  $\beta$  is less than 1. The situation for  $\beta > 1$  needs to be studied in the future. Of course, other mechanisms could not be excluded.

Figure 2 shows the results of superposed epoch analysis for the HCS crossings with a moderate  $\beta$  HPS. As shown in Figure 2(a), typical HCS crossing is identified from the sudden changes of  $\phi_B$  and  $B_X$ . No clear velocity shears are found around the HCS, and the total pressure keeps constant for the entire HCS crossing. Statistically, a 30–40 minutes HPS can be identified around the HCS crossing based on the concurrent decrease of  $B_T$  (from 6 to 4.5 nT) and increase of  $N_{SW}$  (from 13 to  $16 \text{ cm}^{-3}$ ) and  $\beta$  (from 0.65 to 1.5). From Figure 2(b), it is clear that the OR of AWs remains nearly stable (about 61%) in spite of small irregular fluctuations, however, the OR of slow waves has a significant enhancement after the HCS crossing, from 13% in the background solar wind to about 22%. This



**Figure 2.** Results of the superposed epoch analysis for the HCS crossings with a moderate  $\beta$  HPS. The arrangement of the plot is the same as that described in Figure 1.



**Figure 3.** Results of the superposed epoch analysis for the HCS crossings with a low  $\beta$  HPS. The arrangement of the plot is the same as that described in Figure 1.

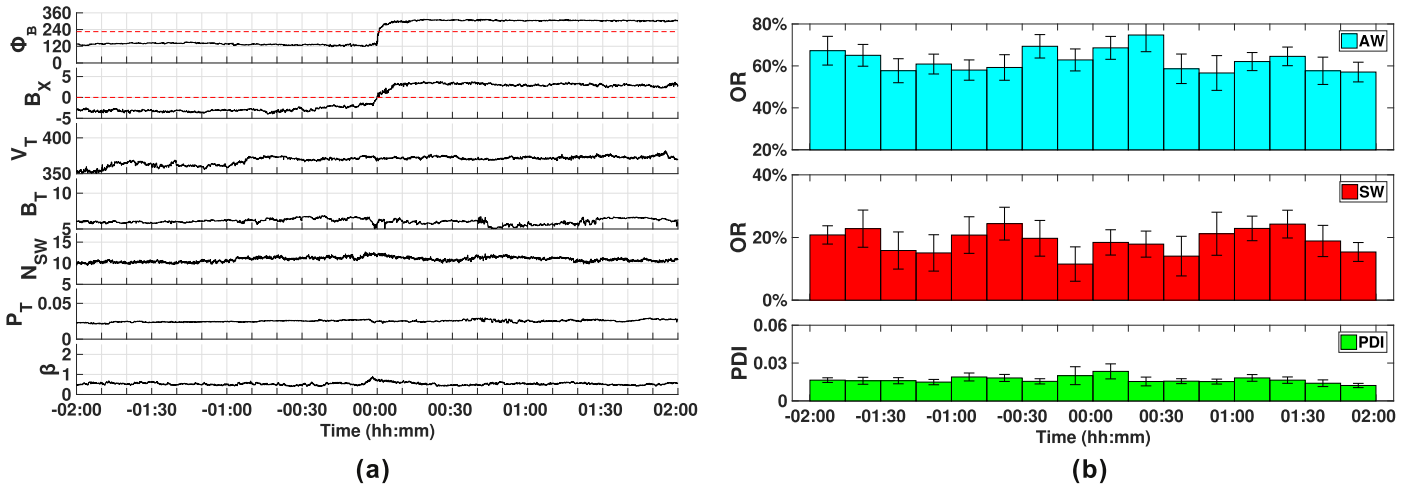


**Figure 4.** Results of the superposed epoch analysis for the HCS crossings without a clear HPS. The arrangement of the plot is the same as that described in Figure 1.

result is in agreement with the simulation results obtained by Malara et al. (1996, 1997).

Figure 3 shows the results of superposed epoch analysis for the HCS crossings with a low  $\beta$  HPS. As shown in Figure 3(a), similarly, typical HCS crossing can be identified from the

sudden change of  $\phi_B$  and  $B_X$ . A minor velocity shear (about  $15 \text{ km s}^{-1}$ ) is found near the HCS crossing. A 30–40 minutes HPS can be identified around the HCS crossing based on the concurrent decrease of  $B_T$  (from 10 to 7.5 nT) and increase of  $N_{SW}$  (from 9 to  $11 \text{ cm}^{-3}$ ) and  $\beta$  (from 0.28 to 0.4). From



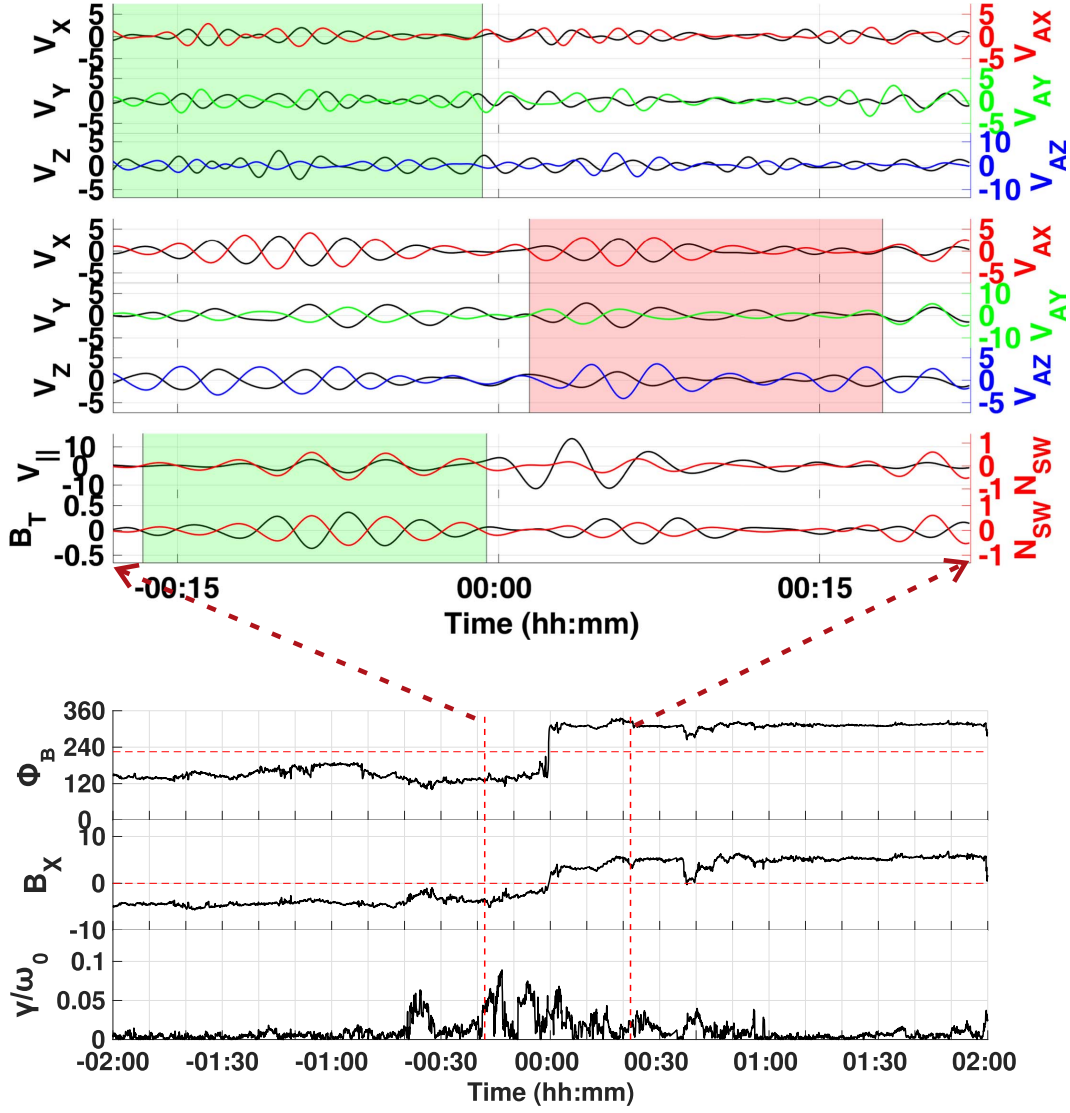


**Figure 5.** Observational clue of PDI during the HCS crossing on 2004 July 19. The top three panels show the AWs with a frequency of 0.01 and 0.005 Hz, and the slow waves with the frequency of 0.005 Hz. The green shaded area denotes the anti-sunward propagating waves, while the red shaded area denotes the sunward propagating waves. The bottom three panels show the profile of  $\phi_B$ ,  $B_x$ , and  $\gamma/\omega_0$ .

Figure 3(b), no obvious regularity can be clearly found for the OR of AWs and slow waves, in spite of small irregular fluctuations. The overall level of the OR of AWs and slow waves is 58% and 20%, respectively.

Figure 4 shows the results of superposed epoch analysis for the HCS crossings without a clear HPS signature. It is clear from Figure 4(a) that  $B_T$ ,  $N_{SW}$ ,  $P_T$ , and  $\beta$  keep invariant in the vicinity of HCS, confirming that there is not a clear HPS structure. Except two small velocity shears in  $-01:45$  and  $-00:52$ ,  $V_T$  remains almost constant during and after the HCS crossing. As shown in Figure 4(b), the results of the OR of the AWs and slow waves are similar to the situations of a low  $\beta$  HPS, except two small enhancements of the OR of slow waves in  $-01:45$  and  $-00:45$  associated with the velocity shears and a 7.8% overall enhancement of the OR of AWs. During the entire HCS crossing, the growth rate of PDI remains at a low level, suggesting that more slow wave generated in the upstream is not due to the PDI of AWs, but is more likely to be the effect of velocity shears in the upstream (Kaghashvili & Esser 2000).

#### 4. Observational Clue of PDI

Although the PDI of AWs in turbulent plasmas have been studied by using 3D MHD simulations and hybrid simulations (Shi et al. 2017; Fu et al. 2018), observational clues of PDI are rarely reported in the literature. As suggested, the PDI of AWs is likely responsible for the enhancement of slow-wave incidence after the HCS crossing with a moderate  $\beta$  HPS. Figure 5 shows an example of observational clues of PDI during the HCS crossing on 2004 July 19. The  $\beta$  of HPS is 1.7, belonging to the moderate  $\beta$  HPS category. The top panel shows the fluctuations in solar wind velocity and Alfvén velocity with the frequency of 0.01 Hz. For the green shaded area before the HCS crossing, all the three component fluctuations negatively correlated, indicating the existence of AWs propagating parallel to the background magnetic field. Considering  $\phi_B$  is about  $147^\circ$ , the AWs propagate anti-sunward. The second panel shows the fluctuations in solar wind velocity and Alfvén velocity with the frequency of 0.005 Hz. For the red shaded area after the HCS crossing, all three component fluctuations negatively correlated as well,

indicating the existence of AWs propagating parallel to the background magnetic field. Considering  $\phi_B$  is about  $312^\circ$ , the AWs propagate sunward. The third panel shows the fluctuations in  $V_{\parallel}$ ,  $N_{SW}$  and  $B$  with the frequency of 0.005 Hz. For the green shaded area before the HCS crossing, the negative correlation between  $\delta B$  and  $\delta N_{SW}$ , together with positive correlation between  $\delta V_{\parallel}$  and  $\delta N_{SW}$ , suggests the existence of slow waves propagating parallel to the background magnetic field. Anti-sunward AWs, sunward AWs, and anti-sunward slow waves co-exist around the HCS crossing when the growth rate of PDI is increasing and lasts for nearly 30 minutes, as shown in the bottom panel. Their wave frequencies satisfy the three-wave resonance condition predicted by the linear theory of parallel PDI ( $\omega_1 = \omega_2 + \omega_3$ ) proposed by Derby (1978) and Goldstein (1978). All the results indicate the occurrence of the PDI of AWs.

To rule out the condition where a sunward AW with the frequency of 0.005 Hz after HCS crossing is caused by the local bending of the IMF line, the criterion proposed by Li et al. (2016a) is adopted: the angles between the background magnetic field of the sunward AW and the upstream/downstream solar wind are both less than  $60^\circ$ . For this case, the angle between the background magnetic field of the sunward AW and the downstream of HCS is calculated to be  $18^\circ$ , satisfying the criterion. In addition, the pitch-angle distribution of suprathermal strahl electrons observed by ACE spacecraft is also checked. The pitch angle of strahl electrons is almost  $180^\circ$  during the AW, indicating the occurrence of a large-scale HCS rather than a local bending of magnetic field line.

Note that there is a peak in the growth rate of PDI of about 35 minutes before the HCS crossing. The outward-propagating AWs and slow waves co-exist at several frequency bands as well, but are not shown here. However, no obvious sunward AWs are found. One plausible reason is that the PDI might not be well developed due to a relative short duration of large growth rate. Further works are needed to explain this phenomenon physically.

## 5. Summary

154 HCSs observed by the *Wind* spacecraft from 1995 to 2013 are analyzed to investigate the properties of associated MHD waves around the HCS crossing. Based on an updated MHD wave detection approach, abundant MHD waves are identified. All the events are divided into four categories: (1) HCS with a high  $\beta$  HPS ( $\beta > 5$ ), 50 cases (32.5%); (2) HCS with a moderate  $\beta$  HPS ( $1 < \beta \leq 5$ ), 55 cases (35.7%); (3) HCS with a low  $\beta$  HPS ( $\beta \leq 1$ ), 19 cases (12.3%); and (4) HCS without a clear HPS, 30 cases (25.7%).

Statistically, plasma  $\beta$  is found to play a key role in the characteristics of MHD waves. For the HCS with a high  $\beta$  HPS, both Alfvén waves and slow waves significantly decay within the HPS, with the OR decreasing by 19% and 6%, respectively. More slow waves are susceptible to attenuation under a higher  $\beta$  conditions, which is in agreement with the prediction made by De Moortel et al. (2004). For the HCS with a moderate  $\beta$  HPS, the OR of Alfvén waves remains nearly stable. However, an enhancement (about 9%) of the OR of slow waves is found after the HCS crossing. The PDI of AWs is suggested to be responsible for the increased excitation of slow waves in the moderate  $\beta$  HPS, and an example of indirect observational clues of PDI is given. For HCS with a low  $\beta$  HPS, the OR of AWs and slow waves remains stable,  $\sim 58\%$  and  $20\%$ , in spite

of some irregular fluctuations. The results for the HCS without a clear HPS are similar to the situations of a low  $\beta$  HPS, although the existence of velocity shear makes the results more complicated. These findings help us to better understand the mode conversion and evolution of MHD waves around the HCS crossing.

The authors thank NASA CDA web (<https://cdaweb.sci.gsfc.nasa.gov/index.html/>) for the *Wind* and *ACE* data. The authors also thank the University of The Wilcox Solar Observatory, for providing the data of the SB list. This work was supported by Strategic Priority Research Program of Chinese Academy of Sciences grant No. XDA17010301), NNSFC grants 41874203, 41574169, 41574159, 41731070, 41204125, Young Elite Scientists Sponsorship Program by CAST, 2016QNRC001, and grants from Chinese Academy of Sciences (QYZDJ-SSW-JSC028, XDA15052500). H. Li was also supported by Youth Innovation Promotion Association of the Chinese Academy of Sciences and in part by the Specialized Research Fund for State Key Laboratories of China.

## ORCID iDs

Hui Li  <https://orcid.org/0000-0002-4839-4614>

Shuo Yao  <https://orcid.org/0000-0003-4267-0486>

## References

- Barnes, A. 1966, *PhFI*, 9, 1483  
 Barnes, A. 1979, *JGR*, 84, 4459  
 Barnes, A., & Hung, R. J. 1972, *JPIPh*, 8, 197  
 Behannon, K. W., Neubauer, F. M., & Barnstorff, H. 1981, *JGR*, 86, 3273  
 Belcher, J. W., & Davis, L. 1971, *JGR*, 76, 3534  
 Blanco, J. J., Rodríguez-Pacheco, J., Hidalgo, M. A., et al. 2006, *JASTP*, 68, 2173  
 Chandran, B. D. G., & Hollweg, J. V. 2009, *ApJ*, 707, 1659  
 Cranmer, S. R., & van Ballegooijen, A. A. 2012, *ApJ*, 754, 92  
 Crooker, N. U., Huang, C.-L., Lamassa, S. M., et al. 2004, *JGRA*, 109, A03107  
 Crooker, N. U., Siscoe, G. L., Shodhan, S., et al. 1993, *JGR*, 98, 9371  
 Dai, L., Wygant, J. R., Cattell, C. A., et al. 2014, *GeoRL*, 41, 1398  
 De Moortel, I., Hood, A. W., Gerrard, C. L., et al. 2004, *A&A*, 425, 741  
 Derby, N. F. 1978, *ApJ*, 224, 1013  
 Du, J., Zhang, T. L., Nakamura, R., et al. 2011, *GeoRL*, 38, L07101  
 Foullon, C., Lavraud, B., Wardle, N. C., et al. 2009, *SoPh*, 259, 389  
 Fu, X., Li, H., Guo, F., Li, X., & Roytershteyn, V. 2018, *ApJ*, 855, 139  
 Galeev, A. A., & Oraevskii, V. N. 1963, *SPhD*, 7, 988  
 Goldstein, M. L. 1978, *ApJ*, 219, 700  
 He, J., Tu, C., Marsch, E., et al. 2015, *ApJL*, 813, L30  
 Kaghshvili, E. Kh., & Esser, R. 2000, *ApJ*, 539, 463  
 Lepping, R. P., Acuña, M. H., Burlaga, L. F., et al. 1995, *SSRv*, 71, 207  
 Li, H., Wang, C., Belcher, J. W., He, J., & Richardson, J. D. 2016a, *ApJL*, 824, L2  
 Li, H., Wang, C., Chao, J. K., et al. 2016b, *JGRA*, 121, 42  
 Li, H., Wang, C., He, J., et al. 2016c, *ApJL*, 831, L13  
 Li, H., Wang, C., Richardson, J. D., & Tu, C. 2017, *ApJL*, 851, L2  
 Lin, R. P., Anderson, K. A., Ashford, S., et al. 1995, *SSRv*, 71, 125  
 Liu, Y. C.-M., Huang, J., Wang, C., et al. 2014, *JGRA*, 119, 8721  
 Malara, F., Primavera, L., & Veltri, P. 1996, *JGR*, 101, 21597  
 Malara, F., Veltri, P., & Primavera, L. 1997, *PhRvE*, 56, 3508  
 Ness, N. F., & Wilcox, J. M. 1964, *PhRvL*, 13, 461  
 Ness, N. F., & Wilcox, J. M. 1965, *Sci*, 148, 1592  
 Owen, C., Alexeev, I. V., Marchaudon, A., et al. 2005, in Proc. Solar Wind 11/SOHO 16, Connecting Sun and Heliosphere, ed. B. Fleck, T. H. Zurbuchen, & H. Lacoste (Paris: ESA), 265  
 Owens, M. J., Crooker, N. U., & Lockwood, M. 2013, *JGRA*, 118, 1868  
 Peng, J., Liu, Y. C.-M., Huang, J., et al. 2017, *JGRA*, 122, 9803  
 Roberts, D. A., Ghosh, S., Goldstein, M. L., et al. 1991, *PhRvL*, 67, 3741  
 Roberts, D. A., Goldstein, M. L., Matthaeus, W. H., et al. 1992, *JGR*, 97, 17115

- Sagdeev, R. Z., & Galeev, A. A. 1969, *Nonlinear Plasma Theory* (New York: Benjamin)
- Schulz, M. 1973, *Ap&SS*, **24**, 371
- Shi, M., Li, H., Xiao, C., & Wang, X. 2017, *ApJ*, **842**, 63
- Shi, M. J., XIAO, C. J., LI, Q. S., et al. 2015, *ApJ*, **815**, 122
- Smith, E. J. 2001, *JGR*, **106**, 15819
- Smith, E. J., & Zhou, X. 2007, in *AIP Conf Proc.* 932, *Turbulence and Nonlinear Processes in Astrophysical Plasmas* (Melville, NY: AIP), 144
- Stribling, T., Roberts, D. A., & Goldstein, M. L. 1996, *JGR*, **101**, 27603
- Tu, C.-Y., & Marsch, E. 1995, *SSRv*, **73**, 1
- Veltri, P., Malara, F., & Primavera, L. 1992, in *Solar Wind Seven*, ed. E. Marsch & R. Schwenn (Oxford: Pergamon), 559
- Winterhalter, D., Smith, E. J., Burton, M. E., et al. 1994, *JGR*, **99**, 6667
- Zhang, L., Yang, L.-P., He, J.-S., et al. 2015, *AnGeo*, **33**, 13